GRADIENT APPROACH TO THE SPHALERON BARRIER

Guido Nolte
Fachbereich Physik, Universität Oldenburg, Postfach 2503
D-26111 Oldenburg, Germany

Jutta Kunz
Fachbereich Physik, Universität Oldenburg, Postfach 2503
D-26111 Oldenburg, Germany
and
Instituut voor Theoretische Fysica, Rijksuniversiteit te Utrecht
NL-3508 TA Utrecht, The Netherlands

February 1, 2008

Abstract

We apply the gradient approach to obtain a path over the sphaleron barrier and to demonstrate the fermionic level crossing phenomenon. Neglecting the mixing angle dependence and assuming that the fermions of a doublet are degenerate in mass we employ spherically symmetric ansätze for the fields. The gradient path over the barrier is smooth, even for large values of the Higgs boson mass or of the fermion mass, where the extremal energy path bifurcates.

Utrecht-Preprint THU-94/14

1 Introduction

In 1976 't Hooft [1] observed that the standard model does not absolutely conserve baryon and lepton number due to the Adler-Bell-Jackiw anomaly. The process 't Hooft considered was spontaneous fermion number violation due to instanton induced transitions. Fermion number violating tunneling transitions between topologically distinct vacua might indeed be observable at high energies at future accelerators [2, 3].

Manton considered the possibility of fermion number violation in the standard model from another point of view [4]. Investigating the topological structure of the configuration space of the Weinberg-Salam theory, Manton showed that there are noncontractible loops in configuration space, and predicted the existence of a static, unstable solution of the field equations, a sphaleron [5], representing the top of the energy barrier between topologically distinct vacua.

At finite temperature this energy barrier between topologically distinct vacua can be overcome due to thermal fluctuations of the fields, and fermion number violating vacuum to vacuum transitions involving changes of baryon and lepton number can occur. The rate for such baryon number violating processes is largely determined by a Boltzmann factor, containing the height of the barrier at a given temperature and thus the energy of the sphaleron. Baryon number violation in the standard model due to such transitions over the barrier may be relevant for the generation of the baryon asymmetry of the universe [6, 7, 8, 9, 10].

While the barrier between topologically distinct vacua is traversed, the Chern-Simons number changes continuously from $N_{\rm CS} = 0$ in one vacuum sector to $N_{\rm CS} \pm 1$ in the neighbouring vacuum sectors, passing through the sphaleron at $N_{CS} = \pm\frac{1}{2}$ [11, 12]. However, for large values of the Higgs boson mass, energetically lower, asymmetric sphaleron solutions appear, the bisphalerons [13, 14]. The minimum energy path over the barrier [11] then develops bifurcations [12], indicating the need for another approach to the sphaleron barrier, which yields smooth paths.

As the barrier is traversed one occupied fermion level crosses from the positive continuum to the negative continuum or vice versa, leading to the change in fermion number. When considered in the background field approximation this level crossing phenomenon predicts the existence of a fermion zero mode precisely at the top of the barrier, at the sphaleron [15, 16, 17]. For massless fermions this zero mode is known analytically [15, 16].

Considering the minimum energy path over the barrier [11, 12] the fermionic level crossing was demonstrated recently in the background field approximation under the assumption, that the fermions of a doublet are degenerate in mass [18, 19, 20]. This assumption, violated in the standard model, allows for spherically symmetric ansätze for all of the fields, when the mixing angle dependence is neglected (which is an excellent approximation [21, 22]). An analogous, but selfconsistent calculation [23] led to similar results. However, for heavy fermions it led to strongly deformed barriers, eventually giving rise to bifurcations and to new sphalerons [23].

Motivated by the catastrophes encountered along the energy barrier in the extremal

energy path approach for large Higgs boson or fermion masses we here consider the gradient approach to the sphaleron barrier. In section 2 we briefly review the Weinberg-Salam Lagrangian and the anomalous currents for vanishing mixing angle and for degenerate fermion doublets. In section 3 we discuss the sphaleron barriers. We present the radially symmetric ansatz for the boson fields and obtain the energy functional. We discuss the gradient approach, putting special emphasis on the question of the underlying metric. We compare the barriers obtained with gradient approach with those of the extremal energy path approach. In section 4 we discuss the fermionic level crossing along the gradient path over the barrier. We present our conclusions in section 5.

2 Weinberg-Salam Lagrangian

We consider the bosonic sector of the Weinberg-Salam theory in the limit of vanishing mixing angle. In this limit the U(1) field decouples and can consistently be set to zero

$$\mathcal{L}_{\rm b} = -\frac{1}{4}F^a_{\mu\nu}F^{\mu\nu,a} + (D_\mu\Phi)^\dagger(D^\mu\Phi) - \lambda(\Phi^\dagger\Phi - \frac{1}{2}v^2)^2 \tag{1}$$

with the $\mathrm{SU}(2)_L$ field strength tensor

$$F^a_{\mu\nu} = \partial_\mu V^a_\nu - \partial_\nu V^a_\mu + g\epsilon^{abc}V^b_\mu V^c_\nu \ , \tag{2}$$

and the covariant derivative for the Higgs field

$$D_\mu\Phi = \Big(\partial_\mu - \frac{1}{2}ig\tau^a V^a_\mu\Big)\Phi \ . \tag{3}$$

The $\mathrm{SU}(2)_{\rm L}$ gauge symmetry is spontaneously broken due to the non-vanishing vacuum expectation value v of the Higgs field

$$\langle\Phi\rangle = \frac{v}{\sqrt{2}}\begin{pmatrix} 0 \\ 1 \end{pmatrix} \ , \tag{4}$$

leading to the boson masses

$$M_W = M_Z = \frac{1}{2}gv \ , \qquad M_H = v\sqrt{2\lambda} \ . \tag{5}$$

We employ the values $M_W = 80$ GeV, $g = 0.65$.

For vanishing mixing angle, considering only fermion doublets degenerate in mass, the fermion Lagrangian reads

$$\begin{aligned} \mathcal{L}_{\rm f} &= \bar{q}_L i\gamma^\mu D_\mu q_L + \bar{q}_R i\gamma^\mu\partial_\mu q_R \\ &- f^{(q)}\bar{q}_L(\tilde{\Phi}u_R + \Phi d_R) - f^{(q)}(\bar{d}_R\Phi^\dagger + \bar{u}_R\tilde{\Phi}^\dagger)q_L \ , \end{aligned} \tag{6}$$

where q_L denotes the lefthanded doublet (u_L, d_L), while q_R abbreviates the righthanded singlets (u_R, d_R), with covariant derivative

$$D_\mu q_L = \Big(\partial_\mu - \frac{1}{2} i g \tau^a V_\mu^a\Big) q_L \ , \tag{7}$$

and with $\tilde{\Phi} = i\tau_2 \Phi^*$. The fermion mass is given by

$$M_F = \frac{1}{\sqrt{2}} f^{(q)} v \ . \tag{8}$$

Due to the U(1) anomaly baryon number and lepton number are not conserved

$$\partial^\mu j_\mu^{\mathrm{B,L}} = -f_{\mathrm{g}} \partial^\mu K_\mu \ , \tag{9}$$

where

$$K_\mu = \frac{g^2}{16\pi^2} \varepsilon_{\mu\nu\rho\sigma} \mathrm{Tr}(\mathcal{F}^{\nu\rho}\mathcal{V}^\sigma + \frac{2}{3} i g \mathcal{V}^\nu \mathcal{V}^\rho \mathcal{V}^\sigma) \tag{10}$$

($\mathcal{F}_{\nu\rho} = 1/2\tau^i F^i_{\nu\rho}$, $\mathcal{V}_\sigma = 1/2\tau^i V^i_\sigma$) is the Chern-Simons current and f_{g} is the number of generations. In the unitary gauge the topological baryon number Q_{B}, carried by a configuration, is determined by its Chern-Simons number N_{CS},

$$N_{\mathrm{CS}} = \int d^3 r K^0 \ . \tag{11}$$

For the vacua the Chern-Simons number is identical to the integer winding number, while the sphaleron at the top of the barrier carries half integer Chern-Simons number [5].

3 Barriers

Approximations to the sphaleron barrier can be obtained by constructing families of field configurations for the gauge and Higgs boson fields, which interpolate smoothly from one vacuum sector to a neighbouring one. The minimum of all maximum energy configurations encountered along such vacuum to vacuum paths represents the sphaleron [5] or, for large Higgs boson masses, the bisphaleron [13, 14]. Applying the gradient approach, we construct the sphaleron barrier for various Higgs boson masses. We compare these barriers to the ones obtained by constructing the extremal energy path [11, 12].

3.1 Energy Functional

In the limit of vanishing mixing angle the gauge and Higgs boson fields can be parametrized by a spherically symmetric ansatz given by [24]

$$V_i^a = \frac{1 - f_A(r)}{gr} \varepsilon_{aij} \hat{r}_j + \frac{f_B(r)}{gr} (\delta_{ia} - \hat{r}_i \hat{r}_a) + \frac{f_C(r)}{gr} \hat{r}_i \hat{r}_a \ , \tag{12}$$

$$V_0^a = 0 \ , \tag{13}$$

$$\Phi = \frac{v}{\sqrt{2}} \Big(H(r) + i\vec{\tau} \cdot \hat{r} K(r)\Big) \begin{pmatrix} 0 \\ 1 \end{pmatrix} \ , \tag{14}$$

which involves the five radial functions $f_A(r)$, $f_B(r)$, $f_C(r)$, $H(r)$ and $K(r)$.

This ansatz is form-invariant under spherically symmetric gauge transformations with the SU(2) matrix

$$U(\vec{r}) = \exp(i\frac{\Theta(r)}{2}\vec{\tau}\cdot\hat{r}) \ . \tag{15}$$

The functions then transform as

$$\begin{aligned} f_A + if_B &\longrightarrow \exp(i\Theta)(f_A + if_B) \ , \\ f_C &\longrightarrow f_C + r\Theta' \ , \\ H + iK &\longrightarrow \exp(i\frac{\Theta}{2})(H + iK) \ . \end{aligned} \tag{16}$$

The ansatz, Eqs. (12)-(14), leads to the bosonic energy functional

$$\begin{aligned} E_{\rm b} &= \frac{4\pi M_W}{g^2}\int_0^\infty dx\Big[\frac{1}{2x^2}(f_A^2+f_B^2-1)^2 + (f_A' + \frac{f_Bf_C}{x})^2 + (f_B' - \frac{f_Af_C}{x})^2 \\ &+ (K^2+H^2)(1+f_A^2+f_B^2+\frac{f_C^2}{2}) + 2f_A(K^2-H^2) - 4f_BHK \\ &- 2xf_C(K'H - KH') + 2x^2(H'^2+K'^2) + \epsilon x^2(H^2+K^2-1)^2\Big] \ , \end{aligned} \tag{17}$$

where

$$x = M_W r \tag{18}$$

is a dimensionless coordinate, the prime denotes differentiation with respect to x, and

$$\epsilon = \frac{4\lambda}{g^2} = \frac{1}{2}\Big(\frac{M_H}{M_W}\Big)^2 \ . \tag{19}$$

This energy functional has a residual U(1) gauge invariance with respect to the gauge transformation, Eq. (16).

The Chern-Simons number of a given configuration is

$$N_{\rm CS} = \frac{1}{2\pi}\int_0^\infty dx\Big[(f_A^2+f_B^2)(\frac{f_C}{x}-\theta') - (\frac{f_C}{x}-\Theta') - \Big(\sqrt{(f_A^2+f_B^2)}\ \sin(\theta-\Theta)\Big)'\Big] \ , \tag{20}$$

where

$$\theta(x) = \arctan(f_B(x)/f_A(x)) \ . \tag{21}$$

The function $\Theta(x)$ is an arbitrary radial function, associated with the U(1) gauge transformation, Eq. (16). From the expression (20) the Chern-Simons number is readily obtained in an arbitrary gauge.

In the radial gauge, where $f_C = 0$, the spatial part of the Chern-Simons current contributes to the topological baryon number. One therefore has to rotate to the unitary gauge, where only the Chern-Simons number determines the topological baryon number.

The corresponding gauge transformation involves the function $\Theta(x)$, which satisfies $\Theta(0) = 0$ and $\Theta(\infty) = \theta(\infty)$. This leads to the Chern-Simons number

$$N_{\rm CS} = \frac{1}{2\pi}\int_0^\infty dx(f_B f_A' - f_A f_B') + \frac{\theta(\infty)}{2\pi} \ . \tag{22}$$

The energy functional, Eq. (17), possesses non-trivial extrema. The sphaleron [5] with $N_{\rm CS} = 1/2$ exists for all Higgs boson masses. For large Higgs boson masses the energetically lower, asymmetric bisphalerons bifurcate from the sphaleron [13, 14].

3.2 Gradient Approach

Let us now consider the energy barriers, associated with the sphaleron and, for large Higgs boson masses, the bisphalerons. For instance, the minimum energy path over the sphaleron barrier is obtained from the functional [11]

$$W = E_{\rm b} + \frac{8\pi^2 M_W}{g^2}\xi N_{\rm CS} \ , \tag{23}$$

where ξ is a dimensionless Lagrange multiplier [11]. This path is satisfactory for small Higgs boson masses [11]. For large Higgs boson masses, however, variation of the functional, Eq. (23), leads to an extremal energy path, which does not culminate at the bisphaleron, but has a spike in the vicinity of the bisphaleron and culminates at the sphaleron [12]. This is in clear contrast to expectation and to other paths constructed in more or less ad hoc fashion [25, 20]. Similarly, when the path is constructed in the presence of fermions with large masses, bifurcations arise along the path in the vicinity of the sphaleron [23].

These catastrophic features of the extremal energy path are artifacts of this approach, indicating the need for another systematic approach to obtain the sphaleron barrier.

3.2.1 Explicit gradient formalism

Let us therefore consider the gradient approach as an alternative approach to the sphaleron barrier. Starting at the sphaleron or bisphaleron we are looking for the steepest path, connecting the top of the barrier with the vacua on both sides.

The direction of steepest descent at the top of the barrier is determined by the negative mode of the sphaleron or bisphaleron [14, 26]. Away from the top of the barrier, the gradient of the energy functional determines the direction of steepest descent. Thus for a given configuration $\tilde{f}$ the neighbouring configuration $f = \tilde{f} + \delta f$ along the path of steepest descent is obtained by choosing δf proportional to the gradient of the energy functional. Explicitly, when f denotes a set of functions f_i, we obtain δf from the functional derivative of the bosonic energy functional $E_{\rm b}$ according to

$$\delta f_i = \alpha\left[\frac{\partial\mathcal{E}(f,f')}{\partial f_i(x)} - \left(\frac{\partial\mathcal{E}(f,f')}{\partial f_i'(x)}\right)'\right]\Bigg|_{f=\tilde{f},f'=\tilde{f}'} \ , \tag{24}$$

with

$$E_{\rm b} = \int dx \mathcal{E}(f_i, f_i') \ , \tag{25}$$

and α is a small negative number.

Metric

The notion "steep" always refers to a metric on the configuration space. Therefore, to unambiguously define the gradient approach, we need to specify a metric on the configuration space. A natural choice for this metric is provided by the kinetic energy term of the Lagrangian [27]. For the spherically symmetric ansatz, Eqs. (12)-(14), the effective mass [28, 29, 30, 31, 32, 33] of the gauge-Higgs-system reads

$$m(\lambda) = \frac{8\pi}{g^2 M_W} \int dx \left[\left(\frac{df_A}{d\lambda}\right)^2 + \left(\frac{df_B}{d\lambda}\right)^2 + \frac{1}{2}\left(\frac{df_C}{d\lambda}\right)^2 + 2x^2\left(\frac{dH}{d\lambda}\right)^2 + 2x^2\left(\frac{dK}{d\lambda}\right)^2 \right] , \tag{26}$$

where λ is an arbitrary path parameter.

Accordingly we define a distance $\hat{d}$ of two configurations $f = (f_A, f_B, f_C, H, K)$ and $\tilde{f} = (\tilde{f}_A, \tilde{f}_B, \tilde{f}_C, \tilde{H}, \tilde{K})$, taken at the "times" λ and $\tilde{\lambda}$, as

$$\begin{aligned} \hat{d}^2(f, \tilde{f}) \ &= \ \frac{16\pi}{g^2} \int dx \Big[(f_A - \tilde{f_A})^2 + (f_B - \tilde{f_B})^2 + \frac{1}{2}(f_C - \tilde{f_C})^2 \\ &\qquad + 2x^2(H - \tilde{H})^2 + 2x^2(K - \tilde{K})^2 \Big] . \end{aligned} \tag{27}$$

Since the gradient formalism assumes a Euclidian metric with equal weight for all indices (i. e. space points and function indices), corresponding to a distance $\hat{d}$

$$\hat{d}^2(f, \tilde{f}) = \frac{16\pi}{g^2} \sum_i \int_0^\infty dx \left(f_i - \tilde{f}_i\right)^2 \ , \tag{28}$$

we have the relations $f_1(x) = f_A(x)$, $f_2(x) = f_B(x)$, $f_3(x) = \frac{1}{\sqrt{2}} f_C(x)$, $f_4(x) = \sqrt{2} x H(x)$ and $f_5(x) = \sqrt{2} x K(x)$.

Equations

Assuming the old configuration $\tilde{f} = (\tilde{f}_A, \tilde{f}_B, \tilde{f}_C, \tilde{H}, \tilde{K})$ is in the radial gauge, $\tilde{f}_C = 0$, the new configuration $f = (f_A, f_B, f_C, H, K)$ will in general not be in the radial gauge, $f_C \neq 0$. Denoting $\delta f = f - \tilde{f}$, we find the set of equations

$$\delta f_A = 2\alpha \Big[\frac{\tilde{f}_A}{x^2}(\tilde{f}_A^2 + \tilde{f}_B^2 - 1) - \tilde{f}_A'' + \tilde{f}_A(\tilde{K}^2 + \tilde{H}^2) + \tilde{K}^2 - \tilde{H}^2 \Big] \ , \tag{29}$$

$$\delta f_B = 2\alpha \Big[\frac{\tilde{f}_B}{x^2}(\tilde{f}_A^2 + \tilde{f}_B^2 - 1) - \tilde{f}_B'' + \tilde{f}_B(\tilde{K}^2 + \tilde{H}^2) - 2\tilde{H}\tilde{K} \Big] \ , \tag{30}$$

$$\delta f_C = \frac{4\alpha}{x} \Big[\tilde{f}_A' \tilde{f}_B - \tilde{f}_B' \tilde{f}_A - x^2(\tilde{K}'\tilde{H} - \tilde{H}'\tilde{K}) \Big] \ , \tag{31}$$

$$\delta H = \frac{\alpha}{x^2}\Big[\tilde{H}(1+\tilde{f}_A^2+\tilde{f}_B^2) - 2\tilde{f}_A\tilde{H} - 2\tilde{f}_B\tilde{K} + 2\tilde{H}\epsilon x^2(\tilde{H}^2+\tilde{K}^2-1) - (2x^2\tilde{H}')'\Big] \ , \quad (32)$$

$$\delta K = \frac{\alpha}{x^2}\Big[\tilde{K}(1+\tilde{f}_A^2+\tilde{f}_B^2) + 2\tilde{f}_A\tilde{K} - 2\tilde{f}_B\tilde{H} + 2\tilde{K}\epsilon x^2(\tilde{H}^2+\tilde{K}^2-1) - (2x^2\tilde{K}')'\Big] \ . \quad (33)$$

To obtain the new configuration in the radial gauge, $\hat{f} = (\hat{f}_A, \hat{f}_B, \hat{f}_C, \hat{H}, \hat{K})$, we perform a gauge transformation, Eq. (16), of $f = (f_A, f_B, f_C, H, K)$ with the gauge function Φ determined by $\hat{f}_C = 0 = f_C + x\Phi'$.

3.2.2 Gradient formalism with constraint

Let us now consider a modified gradient formalism, which is equivalent to the explicit gradient approach in the limit $\hat{d}(f,\tilde{f}) \to 0$. In the explicit gradient formalism the gradient is taken at the 'old' configuration $\tilde{f}$. In the modified gradient formalism we take the gradient at the 'new' configuration $f = \tilde{f} + \delta f$. Then Eq. (24) is a set of differential equations for the functions f_i, which can also be obtained by variation of the functional W

$$W(f) = E_{\rm b}(f) + \frac{1}{4}\xi M_W \hat{d}^2(f,\tilde{f}) \ , \quad (34)$$

where a constraint is imposed on the distance $\hat{d}(f,\tilde{f})$, and ξ is a Lagrange multiplier inverse proportional to α.

Choice of gauge

As before, starting from a configuration in the radial gauge, $\tilde{f}_C = 0$, the neighbouring configuration will in general not be in the radial gauge, $f_C \neq 0$. To be able to keep the radial gauge throughout, we define a new distance $d(f,\tilde{f})$

$$\begin{aligned} &d(f,\tilde{f}) = \min_\Phi \hat{d}(f,\tilde{f}_{-\Phi}) = \\ &\Bigg\{\frac{16\pi}{g^2}\min_\Phi \int dx \Big[\Big(f_A - (\tilde{f}_A\cos(\Phi) + \tilde{f}_B\sin(\Phi))\Big)^2 + \Big(f_B - (\tilde{f}_B\cos(\Phi) - \tilde{f}_A\sin(\Phi))\Big)^2 \\ &+2x^2\Big(H - (\tilde{H}\cos(\Phi/2) + \tilde{K}\sin(\Phi/2))\Big)^2 + 2x^2\Big(K - (\tilde{K}\cos(\Phi/2) - \tilde{H}\sin(\Phi/2))\Big)^2 \\ &+\frac{1}{2}\Big(f_C - \tilde{f}_C + x\Phi'\Big)^2\Big]\Bigg\}^{1/2} \ , \end{aligned} \quad (35)$$

where $\tilde{f}_\Phi$ is obtained by gauge transforming $\tilde{f}$ with the gauge function Φ, which minimizes the distance (35). In contrast with the distance, Eq. (27), the new distance is gauge invariant under independent gauge transformations of f and $\tilde{f}$. (Denoting the configuration space by C, this is a proper metric on the projective space of gauge orbits $C/\sim$, where the equivalence relation $\sim$ identifies configurations which are connected by radially symmetric gauge transformations, Eq. (16) [34].)

Equations

Variation of the functional W, Eq. (34), with distance $\hat{d}(f,\tilde{f})$ replaced by $d(f,\tilde{f})$ leads in the gauge $f_C = \tilde{f}_C = 0$ for the gauge and Higgs field functions to the set of equations

$$f_A'' = \frac{f_A}{x^2}(f_A^2+f_B^2-1) + f_A(K^2+H^2) + K^2 - H^2 + \xi\Big(f_A - (\tilde{f}_A\cos(\Phi) + \tilde{f}_B\sin(\Phi))\Big) \ , \quad (36)$$

$$f_B'' = \frac{f_B}{x^2}(f_A^2 + f_B^2 - 1) + f_B(K^2 + H^2) - 2HK + \xi\left(f_B - (\tilde{f}_B\cos(\Phi) - \tilde{f}_A\sin(\Phi))\right) \ , \quad (37)$$

$$\begin{aligned} H'' &= -\frac{2}{x}H' + \frac{H}{2x^2}\Big((1-f_A)^2 + f_B^2\Big) - \frac{K}{x^2}f_B + (H^2 + K^2 - 1)H \\ &+ \xi\left(H - (\tilde{H}\cos(\Phi/2) + \tilde{K}\sin(\Phi/2))\right) \ , \end{aligned} \quad (38)$$

$$\begin{aligned} K'' &= -\frac{2}{x}K' + \frac{K}{2x^2}\Big((1+f_A)^2 + f_B^2\Big) - \frac{H}{x^2}f_B + \epsilon(H^2 + K^2 - 1)K \\ &+ \xi\left(K - (\tilde{K}\cos(\Phi/2) - \tilde{H}\sin(\Phi/2))\right) \ , \end{aligned} \quad (39)$$

and to an additional equation for Φ

$$\begin{aligned} \Phi'' &= -\frac{2}{x}\Phi' + \frac{2}{x^2}\sin(\Phi)(f_A\tilde{f}_A + f_B\tilde{f}_B) + \frac{2}{x^2}\cos(\Phi)(f_B\tilde{f}_A - f_A\tilde{f}_B) \\ &+2\sin(\Phi/2)(H\tilde{H} + K\tilde{K}) + 2\cos(\Phi/2)(K\tilde{H} - H\tilde{K}) \ . \end{aligned} \quad (40)$$

Boundary conditions

The boundary conditions are chosen such that both the energy density and the energy are finite. At the origin the gauge and Higgs field functions satisfy the boundary conditions

$$f_A(0) - 1 = f_B(0) = H'(0) = K(0) = 0 \ . \quad (41)$$

At infinity the gauge and Higgs field functions lie on a circle

$$f_A(\infty) + if_B(\infty) = \exp(i\theta(\infty)) \ , \quad H(\infty) + iK(\infty) = \exp(i\frac{\theta(\infty)}{2}) \ , \quad (42)$$

where $\theta(\infty)$ is an unknown function of ξ. Therefore we choose the boundary conditions

$$f_A'(\infty) = f_B'(\infty) = H'(\infty) = K'(\infty) = 0 \ . \quad (43)$$

For the gauge function Φ we choose the boundary conditions

$$\Phi(0) = 0 \ , \quad \Phi'(\infty) = 0 \ , \quad (44)$$

consistent with the boundary conditions of the gauge and Higgs field functions.

3.3 Results

In the calculations presented we have employed the gradient formalism with constraint on the distance, since it appeared numerically far more stable than the explicit gradient approach. Let us now discuss the sphaleron barrier as obtained in the gradient approach.

Barrier

We first compare the gradient path with the minimum energy path for small Higgs boson masses. In Fig. 1 we show the energy as a function of the Chern-Simons number for $M_H = M_W$ for the gradient path and the minimum energy path. The minimum energy path barrier is steeper with respect to the Chern-Simons number than the gradient path barrier. This picture reverts, when we consider the energy as a function of the pathlength l, defined by

$$l = \int_{vacuum}^{f} df - \int_{vacuum}^{(bi)sphaleron} df \ . \tag{45}$$

Note, that the pathlength l is shifted such that the sphaleron or bisphaleron has $l = 0$. In Fig. 2 we show the energy as a function of the pathparameter l for $M_H = M_W$ along the gradient path and the minimum energy path. With respect to the pathparameter l the gradient barrier is steeper.

In Fig. 3 we present two configurations with the same Chern-Simons number, one along the gradient path and one along the minimum energy path. For the latter configuration the asymptotic values of the functions are already closer to the vacuum values.

In Fig. 4 we show the energy, obtained with the gradient method, as a function of the Chern-Simons number for $M_H = 15M_W$. Now there are three extrema of the energy functional, the two degenerate bisphalerons and the symmetric sphaleron. The right bisphaleron barrier is obtained from the left one by the transformation $N_{\rm CS} \to 1 - N_{\rm CS}$ and $E \to E$. All three barriers, the lower asymmetric bisphaleron barriers and the higher symmetric sphaleron barrier, are smooth in the gradient approach, in contrast with the bifurcations encountered along the extremal energy path. Note, that the asymmetric bisphaleron barrier culminates at the bisphaleron and has on one side a very steep fall-off [36]. In Fig. 5 we show these energy barriers as functions of the pathparameter l.

The effective mass m is shown in Fig. 6 as a function of the Chern-Simons number for $M_H = M_W$ and $M_H = 15M_W$. For small Higgs boson masses, we find a smooth effective mass, qualitatively similar to [30]. But for large Higgs boson masses the effective mass develops a sharp peak, when the Higgs field crosses zero at spatial origin. This point coincides with the symmetric sphaleron, but not with the bisphaleron. In the vicinity of this peak the potential energy falls off steeply. This steep fall-off occurs only on one side (the side of the peak) of the bisphaleron, but on both sides of the symmetric sphaleron.

By computing the distance of the (symmetric) sphaleron to the vacuum we obtain an estimate of how good the paths are. For $M_H = M_W$ the distance is 40, while the pathlength of the gradient path is 46, and the pathlength of the minimum energy path is 50. Thus the minimum energy path has a longer pathlength than the gradient path.

Tunneling amplitude

As a related criterion for the quality of a path let us now consider the associated semiclassical tunneling amplitude, determined by $\exp(-R_0)$ [28, 29, 30, 31, 32, 33]

$$R_0 = \int_a^b d\lambda \sqrt{2m(\lambda)(V(\lambda) - E)} \ , \tag{46}$$

where $V(\lambda)$ is the potential energy and E is the energy of the classical turning points a and b [30, 31]. (Note that the integral is independent of a reparametrization.) Considering

vacuum to vacuum transitions, (with respect to the above metric, Eq. (27),) the exponent R_0 of the tunneling amplitude is a line integral along the path in configuration space,

$$R_0 = \int_a^b \hat{d}f \, \sqrt{\frac{E_b(f)}{M_W}} \ , \tag{47}$$

where

$$\hat{d}f = \lim_{\tilde{f}\to f} \hat{d}(f,\tilde{f}) \ , \tag{48}$$

$V(\lambda) = E_{\rm b}$, and $E = 0$. Employing the radial gauge in the calculations, the tunneling amplitude is determined by R_0 as given in Eq. (47) with $\hat{d}(f,\tilde{f})$, Eq. (27), replaced by $d(f,\tilde{f})$, Eq. (35), where we now interpret the sequence of configurations along the path as gauge transforms of those configurations for which $d(f,\tilde{f})$ equals $\hat{d}(f,\tilde{f})$.

For $M_H = M_W$ we find $R_0 = 1.575$ and 1.836, in units of $\frac{8\pi^2}{g^2}$, for the gradient path and the minimum energy path, respectively. For $M_H = 15M_W$ we find $R_0 = 1.525$ (1.533), in units of $\frac{8\pi^2}{g^2}$, for the bisphaleron barrier (symmetric sphaleron barrier) in the gradient approach. In Fig. 7 we show R_0 as a function of the Higgs boson mass in the gradient approach. We observe, that $R_0 \approx 1.5$, in units of $8\pi^2/g^2$, fairly independent of the Higgs boson mass, and the bisphaleron transition rate is slightly higher than the sphaleron transition rate.

4 Level Crossing

Let us now consider the fermionic level crossing phenomenon along the sphaleron barrier. We study the fermion mode in the background field of the barrier as well as selfconsistently, and compare the gradient path to the extremal energy path.

4.1 Energy Functional

To retain spherical symmetry we consider only fermion doublets degenerate in mass. The corresponding spherically symmetric ansatz for the fermion eigenstates is the hedgehog ansatz,

$$q_L(\vec{r},t) = e^{-i\omega t} M_W^{\frac{3}{2}} [G_L(r) + i\vec{\sigma}\cdot\hat{r}F_L(r)]\chi_{\rm h} \ , \tag{49}$$

$$q_R(\vec{r},t) = e^{-i\omega t} M_W^{\frac{3}{2}} [G_R(r) - i\vec{\sigma}\cdot\hat{r}F_R(r)]\chi_{\rm h} \ , \tag{50}$$

where the normalized hedgehog spinor $\chi_{\rm h}$ satisfies the spin-isospin relation

$$\vec{\sigma}\chi_{\rm h} + \vec{\tau}\chi_{\rm h} = 0 \ . \tag{51}$$

Under the residual gauge transformation, Eq. 15, the fermion functions transform as

$$\begin{aligned} F_L + iG_L &\longrightarrow \exp(i\frac{\Theta}{2})(F_L + iG_L) \ , \\ F_R + iG_R &\longrightarrow F_R + iG_R \ . \end{aligned} \tag{52}$$

The fermionic energy functional reads

$$\begin{aligned} E_{\rm f} &= 4\pi M_W \int_0^\infty dx x^2 \Big[F_R' G_R - G_R' F_R + \frac{2}{x} F_R G_R + F_L' G_L - G_L' F_L + \frac{2}{x} F_L G_L \\ &- 2\frac{1-f_A}{x} G_L F_L + \frac{f_B}{x}(G_L^2 - F_L^2) + \frac{f_C}{2x}(G_L^2 + F_L^2) \\ &+ 2\tilde{M}_F H (G_R G_L - F_R F_L) - 2\tilde{M}_F K (F_R G_L + F_L G_R) \Big] \ , \end{aligned} \tag{53}$$

where the fermion mass M_F is expressed in units of M_W

$$\tilde{M}_F = M_F / M_W \ . \tag{54}$$

The fermion functions need to be normalized. When N fermions occupy the eigenstate the normalization condition is

$$4\pi \int_0^\infty dx x^2 (G_R^2 + F_R^2 + G_L^2 + F_L^2) = N \ . \tag{55}$$

4.2 Background Field Calculation

Let us first consider the fermions in the background field of the sphaleron barrier. We find the set of coupled equations [18, 20, 23]

$$\tilde{\omega} G_L - F_L' - \frac{2}{x} F_L + \frac{1-f_A}{x} F_L - \frac{f_B}{x} G_L + \tilde{M}_F (-H G_R + K F_R) = 0 \ , \tag{56}$$

$$\tilde{\omega} F_L + G_L' + \frac{1-f_A}{x} G_L + \frac{f_B}{x} F_L + \tilde{M}_F (H F_R + K G_R) = 0 \ , \tag{57}$$

$$-\tilde{\omega} G_R + F_R' + \frac{2}{x} F_R + \tilde{M}_F (H G_L - K F_L) = 0 \ , \tag{58}$$

$$\tilde{\omega} F_R + G_R' + \tilde{M}_F (H F_L + K G_L) = 0 \ , \tag{59}$$

where $\tilde{\omega}$ is the fermion eigenvalue ω in units of M_W

$$\tilde{\omega} = \frac{\omega}{M_W} \ . \tag{60}$$

At the origin the fermion functions satisfy the boundary conditions

$$F_R(0) = F_L(0) = 0 \ , \tag{61}$$

and

$$G_R(0) = c_R \ , \quad G_L(0) = c_L \ , \tag{62}$$

where c_R and c_L are unknown constants, subject to the normalization condition (55). At infinity all fermion functions vanish

$$F_R(\infty) = F_L(\infty) = G_R(\infty) = G_L(\infty) = 0 \ . \tag{63}$$

Let us now consider the case $M_H = M_W$. The fermion eigenvalue along the gradient path is shown in Fig. 8 as a function of the Chern-Simons number for the fermion masses $M_F = 10M_W$, $M_F = M_W$ and $M_F = M_W/10$. For comparison the fermion eigenvalue along the minimum energy path is also shown [18]. For small fermion masses the fermions are bound only in the vicinity of the sphaleron. Here we find qualitatively the same behaviour of the fermion eigenvalue. For heavier fermions the eigenmode reaches the continua later along the gradient path than along the minimum energy path.

For large values of the Higgs boson mass, when the barrier culminates at the bisphaleron, the fermion eigenvalue in the gradient approach is a monotonic function of the Chern-Simons number as shown in Fig. 9 for $M_H = 15M_W$ and $M_F = 10M_W$, $M_F = M_W$ and $M_F = M_W/10$. This is in contrast with the extremal energy path, where the bifurcations along the path also lead to bifurcations of the fermion eigenvalue [20]. Note, that the eigenvalue along the right bisphaleron barrier is obtained by the transformation $N_{\rm CS} \to 1 - N_{\rm CS}$ and $\omega \to -\omega$.

In Fig. 10 we show the dependence of the zero eigenvalue of the fermions on the Chern-Simons number and on the fermion mass for the gradient path and the extremal energy path for $M_H = 15M_W$. Depending on the Higgs boson mass, the zero mode approaches a limiting value for large fermion masses in the gradient approach. In contrast, along the extremal energy path the zero mode occurs for large fermion masses only at the sphaleron, i. e. at $N_{\rm CS} = 1/2$. For small fermion masses the level crossing occurs for both methods in the vicinity of $N_{\rm CS} = 1/2$ [20, 36].

4.3 Selfconsistent Calculation

Let us now study the gradient path over the sphaleron barrier in the presence of fermions. We proceed analogously to our previous calculation [23], but compute the barrier with the gradient method. We arrive at the same set of equations for the fermion fields, while we have to add the source terms

$$+ g^2 x F_L G_L \ , \tag{64}$$

$$+ \frac{1}{2} g^2 x (G_L^2 - F_L^2) \ , \tag{65}$$

$$+ \frac{g^2 \tilde{M}_F}{2} (G_R G_L - F_R F_L) \ , \tag{66}$$

$$- \frac{g^2 \tilde{M}_F}{2} (F_R G_L + F_L G_R) \ , \tag{67}$$

to the right hand side of the boson field equations for f_A, f_B, H, and K, respectively.

Let us first consider small Higgs boson masses, where only the sphaleron barrier exists. As before, when studying the fermion eigenmode along the minimum energy path [23], we observe that fermions with small masses have little influence on the shape of the barrier, while heavy fermions deform the barrier considerably. However, for very large fermion masses, the bifurcations, which we observed previously along the extremal energy

path, are no longer present along the gradient path. In the gradient approach the barrier decreases monotonically to both sides of the sphaleron, as shown in Fig. 11 for $M_H = M_W$ and $M_F = 75 M_W$.

As before [23] we observe, that the fermion eigenvalue deviates litte from the eigenvalue of the background field calculation for small fermion masses, also for heavier fermions the path does not lead to a free fermion solution but to a bound state, a nontopological soliton. The selfconsistent fermion eigenvalue along the gradient barrier is shown in Fig. 12 for a heavy fermion with $M_F = 10 M_W$ for the Higgs boson mass $M_H = M_W$, and compared to the eigenvalue of the background field calculation. In the selfconsistent calculation the soliton is approached for $N_{\rm CS} \to 0$.

Let us now turn to large values of the Higgs boson mass, where we expect two bisphaleron barriers beside the sphaleron barrier. The presence of the fermions lifts the degeneracy of the two bisphalerons for finite fermion masses. Considering now the total energy, consisting of the bosonic energy and the fermion eigenvalue as encountered along the path over the barrier, we expect [38], that the energy of the left bisphaleron first increases as $E = E_{\rm b} + M_F$, while the energy of the right bisphaleron decreases as $E = E_{\rm b} - M_F$. (The left sphaleron is encountered along the barrier before the level crossing, i. e. the fermion is still in the positive continuum, while the right sphaleron is encountered after the level crossing, i. e. the fermion is in the negative continuum [20].) At a critical value of the fermion mass the fermion becomes bound, $M_F^{cr} \approx 4\sqrt{M_H/M_W - 12}$ GeV [37]. Then the energy of the left bisphaleron decreases, while the energy of the right bisphaleron increases. Interestingly, a bifurcation occurs at a moderate value of the fermion mass. The right bisphaleron merges with the sphaleron at a critical value, beyond which only the left bisphaleron solution exists. This curious feature of the selfconsistent treatment is demonstrated in Fig. 13 for $M_H = 15 M_W$ (for one bound fermion).

The selfconsistent fermion eigenvalue for a heavy fermion with $M_F = 10 M_W$ for the Higgs boson mass $M_H = 15 M_W$ along the left gradient bisphaleron barrier is shown in Fig. 12. Note, that this is the only selfconsistent barrier for this fermion mass. Here, the vacuum is approached for $N_{\rm CS} \to 0$, because the soliton exists only for higher fermion masses [23].

5 Conclusion

We have applied the gradient approach to obtain the sphaleron barrier. The gradient approach produces a path of steepest descent with respect to a given metric. A natural metric on the space of field configurations is implied by the kinetic energy term of the Lagrangian [27]. We have formulated this metric in a gauge invariant way [34].

We have presented the formalism of the explicit gradient approach and of the gradient approach with a constraint on the distance. For technical reasons we have used the latter approach in the numerical calculations.

Since the bifurcations along the extremal energy path have largely motivated this

study, we have compared the sphaleron barrier obtained along the gradient path to the one along the extremal energy path. For small values of the Higgs boson mass, there is only one sphaleron solution, the symmetric sphaleron [5, 13, 14]. Here both approaches lead to a smooth barrier. The gradient path barrier is steeper with respect to the path-length l, defined via the metric, while the minimum energy path is steeper with respect to the Chern-Simons number. But the semiclassically calculated tunneling amplitude, $\sim \exp(-R_0)$, is bigger for the gradient path, e. g. for $M_H = M_W$ R_0 is smaller by 10% for the gradient path.

For Higgs boson masses larger than ~ 1 TeV new asymmetric sphaleron solutions with lower energy appear, the bisphalerons, [13, 14]. When bisphalerons exist, the extremal energy path has bifurcations and culminates not at the bisphaleron but at the symmetric sphaleron. In contrast, the gradient approach leads to smooth barriers, a lower asymmetric bisphaleron barrier and a higher symmetric sphaleron barrier. The asymmetric barrier has a steep fall-off on one side. This fall-off is related to a peak in the effective mass, when the Higgs field passes zero (at the origin). The semiclassical tunneling amplitude is fairly independent of the Higgs boson mass, but slightly bigger along the bisphaleron barrier than along the sphaleron barrier.

To exhibit the level crossing phenomenon we have calculated the valence fermion mode along the gradient approach barriers. Since the barriers are smooth in the gradient approach, also the fermion eigenvalue along the barriers is smooth. This is in contrast to the extremal energy path, where the bifurcations of the barriers were reflected in bifurcations of the fermion eigenvalue [20]. The fermion eigenvalue decreases monotonically from the positive continuum to the negative continuum along the gradient path in the background field approximation, even for large values of the Higgs boson mass.

When fermions are coupled selfconsistently to the boson fields the fermion mass is of importance. For small fermions masses there is hardly any change with respect to the background field calculations, while for heavy fermions the barriers deform considerably. Notably, for large Higgs boson masses, two of the three barriers, the sphaleron barrier and the right bisphaleron barrier, merge and disappear already for moderate values of the fermion mass, leaving as the only barrier the left bisphaleron barrier.

Acknowledegement

We gratefully acknowledge discussions with Y. Brihaye, B. Kleihaus, M. Wendel and L. Yaffe.

References

[1] G. 't Hooft, Symmetry breaking through Bell-Jackiw Anomalies, Phys. Rev. Lett. 37 (1976) 8.

[2] A. Ringwald, Rate of anomalous electroweak baryon and lepton number violation at finite temperature, Phys. Lett. B201 (1988) 510.

[3] M. Mattis, and E. Mottola, eds., "Baryon Number Violation at the SSC?", World Scientific, Singapore (1990).

[4] N. S. Manton, Topology in the Weinberg-Salam theory, Phys. Rev. D28 (1983) 2019.

[5] F. R. Klinkhamer, and N. S. Manton, A saddle-point solution in the Weinberg-Salam theory, Phys. Rev. D30 (1984) 2212.

[6] V. A. Kuzmin, V. A. Rubakov, and M. E. Shaposhnikov, On anomalous electroweak baryon-number non-conservation in the early universe, Phys. Lett. B155 (1985) 36.

[7] P. Arnold, and L. McLerran, Sphalerons, small fluctuations, and baryon-number violation in electroweak theory, Phys. Rev. D36 (1987) 581.

[8] P. Arnold, and L. McLerran, The sphaleron strikes back: A response to objections to the sphaleron approximation, Phys. Rev. D37 (1988) 1020.

[9] L. Carson, X. Li, L. McLerran, and R.-T. Wang, Exact computation of the small-fluctuation determinant around a sphaleron, Phys. Rev. D42 (1990) 2127.

[10] E. W. Kolb, and M. S. Turner, "The Early Universe", Addison-Wesley Publishing Company, Redwood City (1990).

[11] T. Akiba, H. Kikuchi, and T. Yanagida, Static minimum-energy path from a vacuum to a sphaleron in the Weinberg-Salam model, Phys. Rev. D38 (1988) 1937.

[12] Y. Brihaye, S. Giler, P. Kosinski, and J. Kunz, Configuration space around the sphaleron, Phys. Rev. D42 (1989) 2846.

[13] J. Kunz, and Y. Brihaye, New sphalerons in the Weinberg-Salam theory, Phys. Lett. B216 (1989) 353.

[14] L. G. Yaffe, Static solutions of SU(2)-Higgs theory, Phys. Rev. D40 (1989) 3463.

[15] C. R. Nohl, Bound-state solutions of the Dirac equation in extended hadron models, Phys. Rev. D12 (1975) 1840.

[16] J. Boguta, and J. Kunz, Hadroids and sphalerons, Phys. Lett. B154 (1985) 407.

[17] A. Ringwald, Sphaleron and level crossing, Phys. Lett. B213 (1988) 61.

[18] J. Kunz, and Y. Brihaye, Fermions in the background of the sphaleron barrier, Phys. Lett. B304 (1993) 141.

[19] D. Diakonov, M. Polyakov, P. Sieber, J. Schaldach and K. Goeke, Fermion sea along the sphaleron barrier, Phys. Rev. D49 (1994) 6864.

[20] J. Kunz, and Y. Brihaye, Level crossing along sphaleron barriers, Phys. Rev. D50 (1994) 1051.

[21] B. Kleihaus, J. Kunz, and Y. Brihaye, The electroweak sphaleron at physical mixing angle, Phys. Lett. B273 (1991) 100.

[22] J. Kunz, B. Kleihaus, and Y. Brihaye, Sphalerons at finite mixing angle, Phys. Rev. D46 (1992) 3587.

[23] G. Nolte, and J. Kunz, The sphaleron barrier in the presence of fermions, Phys.Rev. D48 (1993) 5905.

[24] R. F. Dashen, B. Hasslacher, and A. Neveu, Nonperturbative methods and extended-hadron models in field theory. III. Four-dimensional non-abelian models, Phys. Rev. D12 (1974) 4138.

[25] F. R. Klinkhamer, Sphalerons, deformed sphalerons and configuration space, Phys. Lett. B236 (1990) 187.

[26] Y. Brihaye and J. Kunz, Normal modes around SU(2) sphalerons, Phys. Lett. B249 (1990) 90.

[27] This choice of metric is within the gradient approach consistent with the requirement of a maximal tunneling rate.

[28] T. Banks, C. M. Bender, and T. T. Wu, Coupled anharmonic oscillators. I. Equal-mass case, Phys. Rev. D8 (1973) 3346.

[29] T. Banks, and C. M. Bender, Coupled anharmonic oscillators. II. Unequal-mass case, Phys. Rev. D8 (1973) 3366.

[30] K. Bitar, and S.-J. Chang, Vacuum tunneling of gauge theory in Minkowsky space, Phys. Rev. D17 (1978) 486.

[31] K. Bitar, and S.-J. Chang, Vacuum tunneling and fluctuations around a most probable escape path, Phys. Rev. D18 (1978) 435.

[32] R. J. Noble, Quantum-field transition rates at finite temperature, Phys. Rev. D20 (1979) 3179.

[33] S. Hsu, On tunneling at finite energies and temperatures, Phys. Lett. B294 (1992) 77.

[34] This metric is a generalization of the Fubini-Study metric [35] to local gauge theory, which is defined for quantum mechanical wavefunctions, which are physically equivalent under a global phase transformation.

[35] A. K. Pati, Relation between "phases" and "distance" in quantum evolution, Phys. Lett. A159 (1991) 105.

[36] Similar results were obtained by L. G. Yaffe, private communication.

[37] Y. Brihaye and J. Kunz, Sphaleron, Fermions and Level Crossing in the Electroweak Model, ICHEP94, Glasgow, July 1994.

[38] Due to the finite radius, we had numerical difficulties to obtain accurate (free fermion) solutions for small fermion masses.

6 Figure Captions

Figure 1: The total energy (in TeV) is shown as a function of the Chern-Simons number $N_{\rm CS}$ along the gradient path (solid) and along the extremal path (dotted) for $M_H = M_W$.

Figure 2: The total energy (in TeV) is shown as a function of the pathparameter l along the gradient path (solid) and along the extremal path (dotted) for $M_H = M_W$.

Figure 3: The gauge field functions f_A and f_B are shown with respect to the dimensionless variable x for the configurations with $N_{\rm CS} = 1/2$ along the gradient path (solid) and along the extremal path (dotted) for $M_H = M_W$.

Figure 4: The total energy (in TeV) is shown as a function of the Chern-Simons number $N_{\rm CS}$ along the symmetric sphaleron path (solid) and along the asymmetric bisphaleron path (dotted) in the gradient approach for $M_H = 15M_W$.

Figure 5: The total energy (in TeV) is shown as a function of the pathparameter l along the symmetric sphaleron path (solid) and along the asymmetric bisphaleron path (dotted) in the gradient approach for $M_H = 15M_W$.

Figure 6: The effective mass (in units of $1/M_W$) is shown as a function of the Chern-Simons number $N_{\rm CS}$ in the gradient approach along the symmetric sphaleron path for $M_H = M_W$ (solid) and $M_H = 15M_W$ (dot-dashed), and along the asymmetric bisphaleron path for $M_H = 15M_W$ (dotted).

Figure 7: The transition amplitude R_0 (in units of $8\pi^2/g^2$) is shown as a function of the Higgs boson mass M_H (in units of M_W) in the gradient approach for the symmetric sphaleron path (solid) and for the asymmetric bisphaleron path (dotted).

Figure 8: The fermion eigenvalue (in units of M_F) is shown as a function of the Chern-Simons number $N_{\rm CS}$ in the background of the sphaleron barrier for the fermion masses $M_F = M_W/10$, $M_F = M_W$ and $M_F = 10M_W$ along the gradient path (solid) and along the extremal path (dotted) for $M_H = M_W$.

Figure 9: The fermion eigenvalue (in units of M_F) is shown as a function of the Chern-Simons number $N_{\rm CS}$ in the background of the bisphaleron barrier for the fermion masses $M_F = M_W/10$, $M_F = M_W$ and $M_F = 10M_W$ along the gradient path (solid) for $M_H = 15M_W$.

Figure 10: For the fermion zero mode the dependence of the fermion mass (in units of M_W) on the Chern-Simons number $N_{\rm CS}$ is shown along the gradient path (solid) and along the extremal path (dotted) for $M_H = 15M_W$.

Figure 11: The energy (in TeV) is shown as a function of the Chern-Simons number $N_{\rm CS}$ for the fermion mass $M_F = 75M_W$ in the selfconsistent calculation along the gradient path (solid) and along the extremal path (dotted) for $M_H = M_W$.

Figure 12: The fermion eigenvalue (in units of M_F) is shown as a function of the Chern-Simons number $N_{\rm CS}$ in the gradient approach along the sphaleron barrier for $M_H = M_W$ and along the bisphaleron barrier for $M_H = 15M_W$ for the fermion mass $M_F = 10M_W$ in the background field calculation (dotted) and in the selfconsistent calculation (solid).

Figure 13: The energy (in TeV), including the fermion eigenvalue, is shown as a function of the fermion mass M_F (in units of M_W) in the selfconsistent calculation for

the left bisphaleron (dotted), for the right bisphaleron (solid), and for the sphaleron (dot-dashed) for $M_H = 15 M_W$.

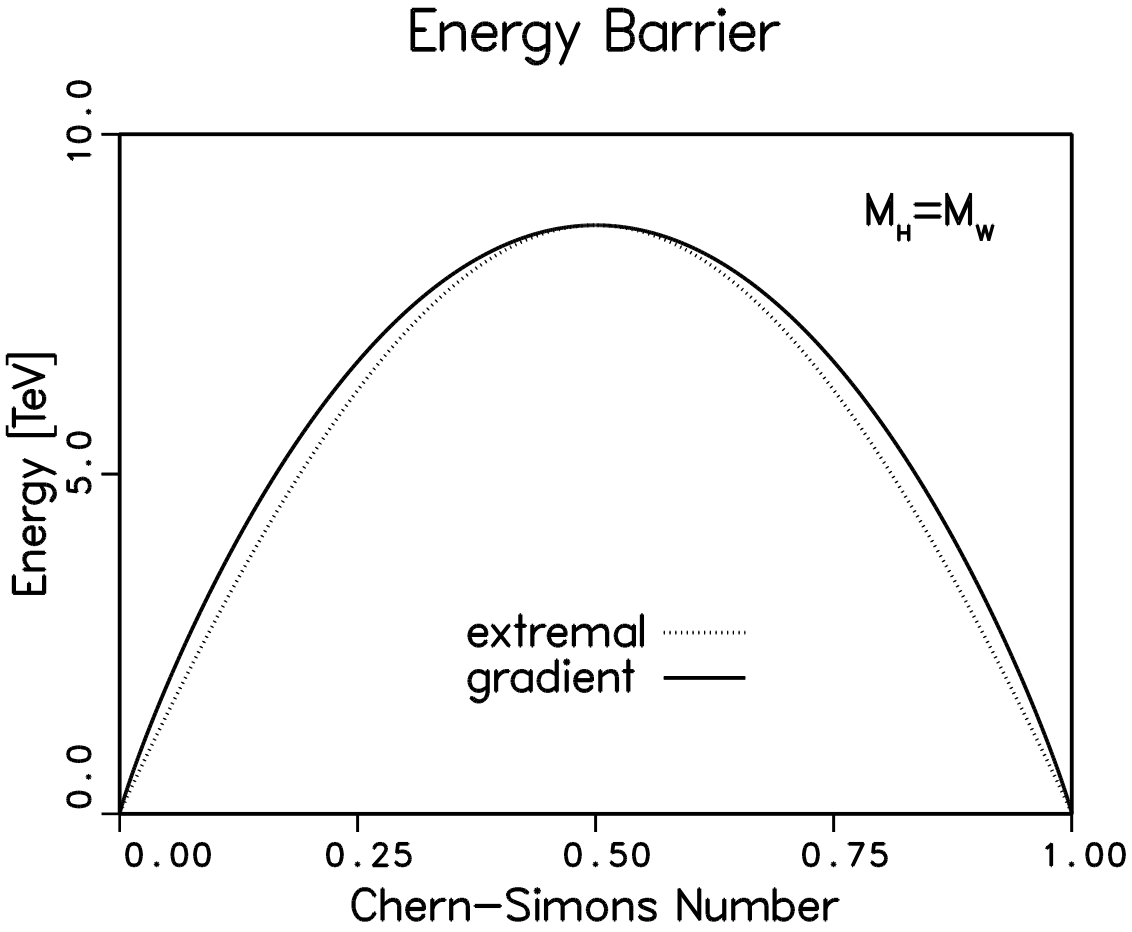
Energy Barrier
10.0
5.0
0.0
Energy [TeV]
$M_H=M_W$
extremal
gradient
0.00
0.25
0.50
0.75
1.00
Chern–Simons Number

This figure "fig1-1.png" is available in "png" format from:

http://arXiv.org/ps/hep-ph/9409445v2

This figure "fig2-1.png" is available in "png" format from:

http://arXiv.org/ps/hep-ph/9409445v2

This figure "fig3-1.png" is available in "png" format from:

http://arXiv.org/ps/hep-ph/9409445v2

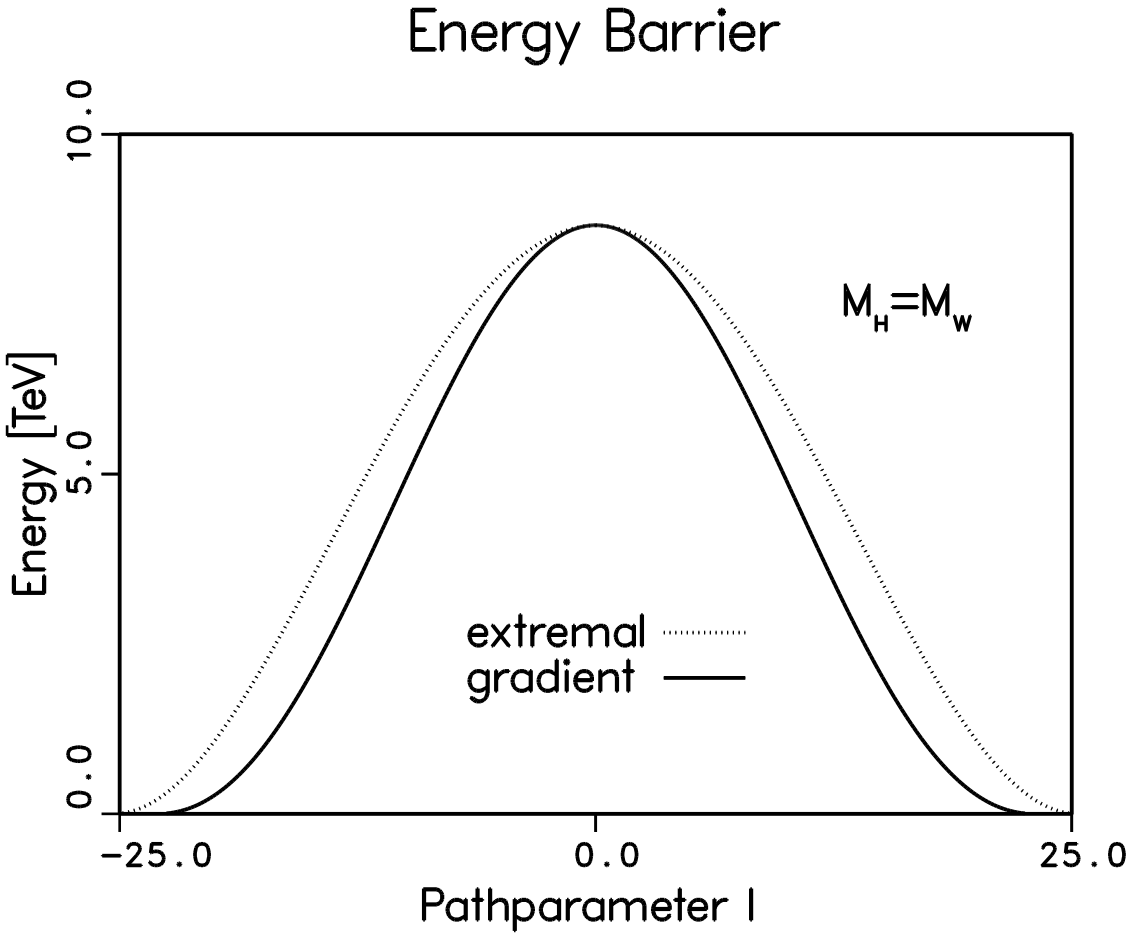
Energy Barrier
10.0
5.0
0.0
Energy [TeV]
$M_H=M_W$
extremal
gradient
−25.0
0.0
25.0
Pathparameter l

This figure "fig1-2.png" is available in "png" format from:

http://arXiv.org/ps/hep-ph/9409445v2

This figure "fig2-2.png" is available in "png" format from:

http://arXiv.org/ps/hep-ph/9409445v2

This figure "fig3-2.png" is available in "png" format from:

http://arXiv.org/ps/hep-ph/9409445v2

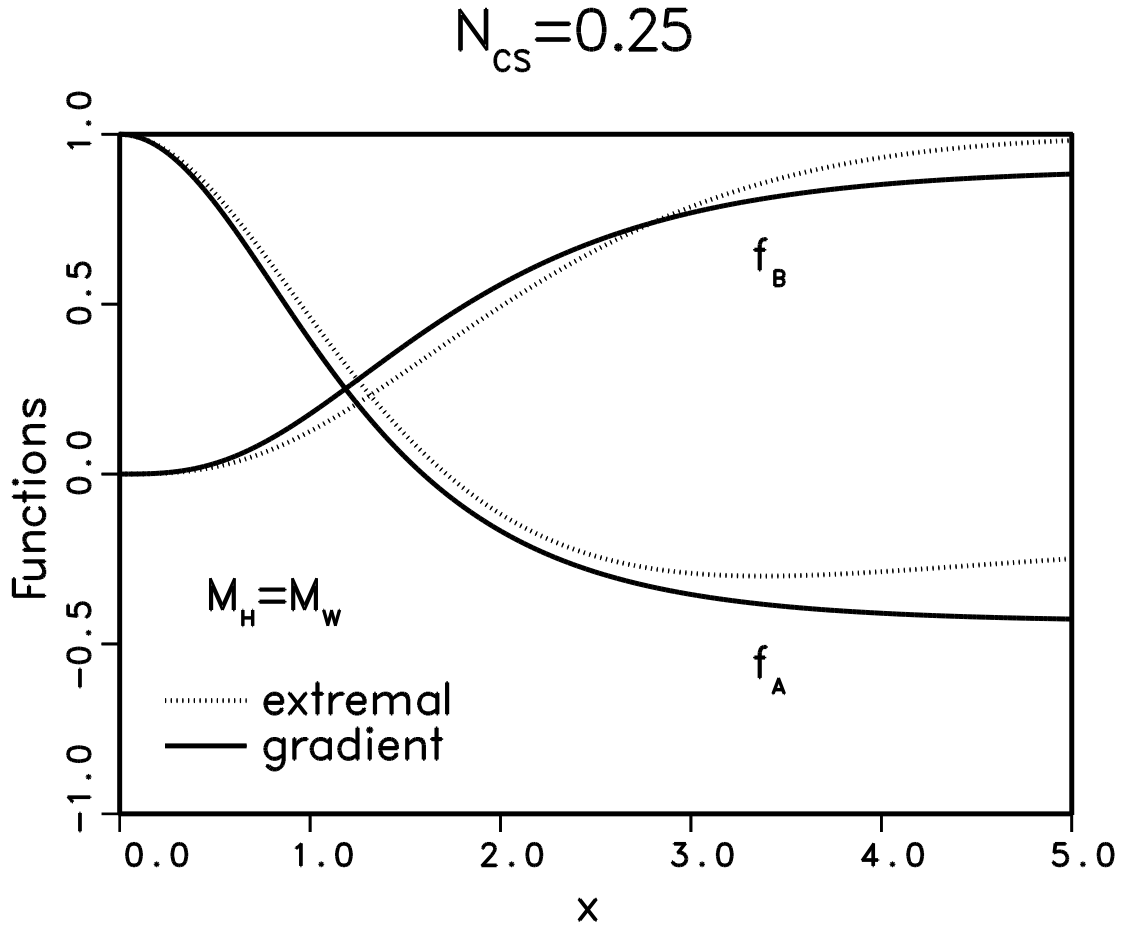
N_{cs}=0.25
Functions
1.0
0.5
0.0
-0.5
-1.0
0.0
1.0
2.0
3.0
4.0
5.0
x
f_B
f_A
M_H=M_W
extremal
gradient

This figure "fig1-3.png" is available in "png" format from:

http://arXiv.org/ps/hep-ph/9409445v2

This figure "fig2-3.png" is available in "png" format from:

http://arXiv.org/ps/hep-ph/9409445v2

This figure "fig3-3.png" is available in "png" format from:

http://arXiv.org/ps/hep-ph/9409445v2

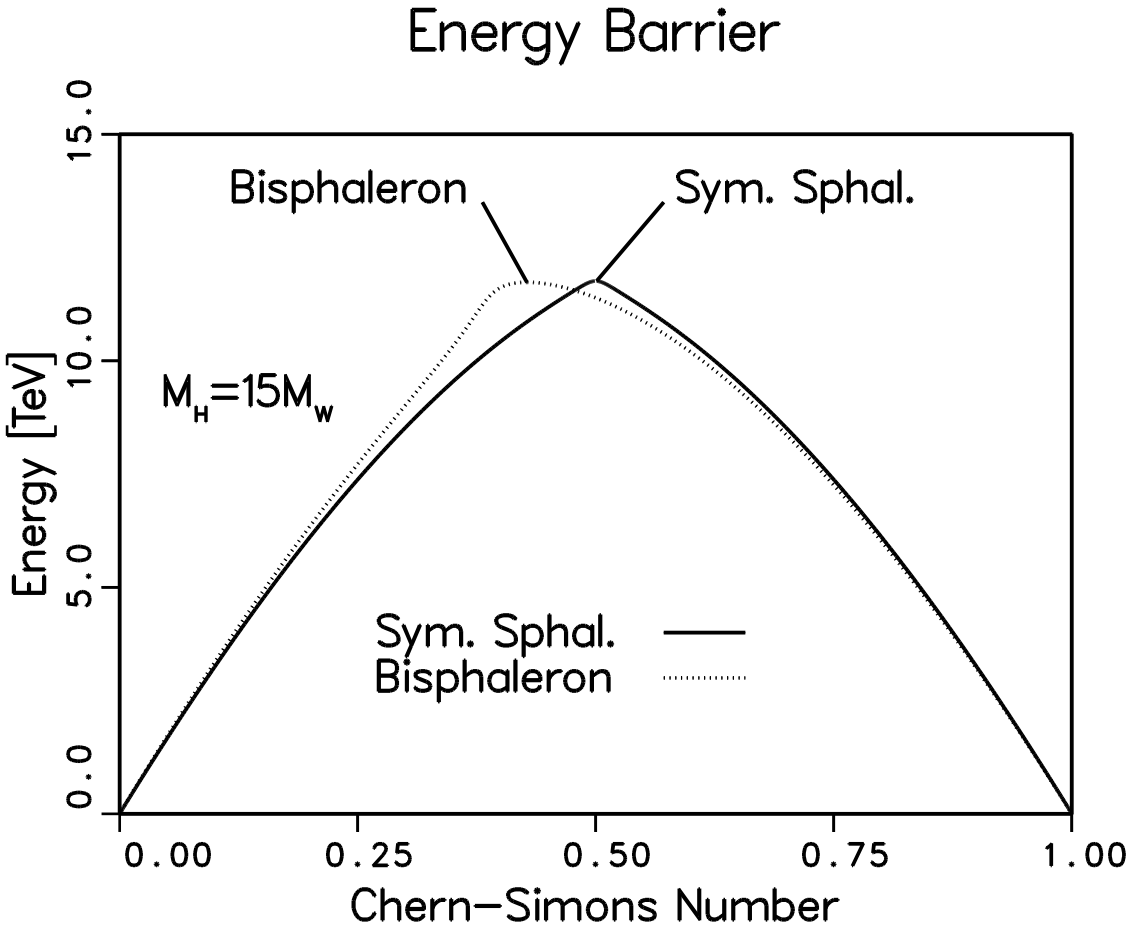
Energy Barrier
Bisphaleron
Sym. Sphal.
$M_H=15M_W$
Sym. Sphal.
Bisphaleron
Energy [TeV]
15.0
10.0
5.0
0.0
0.00
0.25
0.50
0.75
1.00
Chern–Simons Number

This figure "fig1-4.png" is available in "png" format from:

http://arXiv.org/ps/hep-ph/9409445v2

This figure "fig2-4.png" is available in "png" format from:

http://arXiv.org/ps/hep-ph/9409445v2

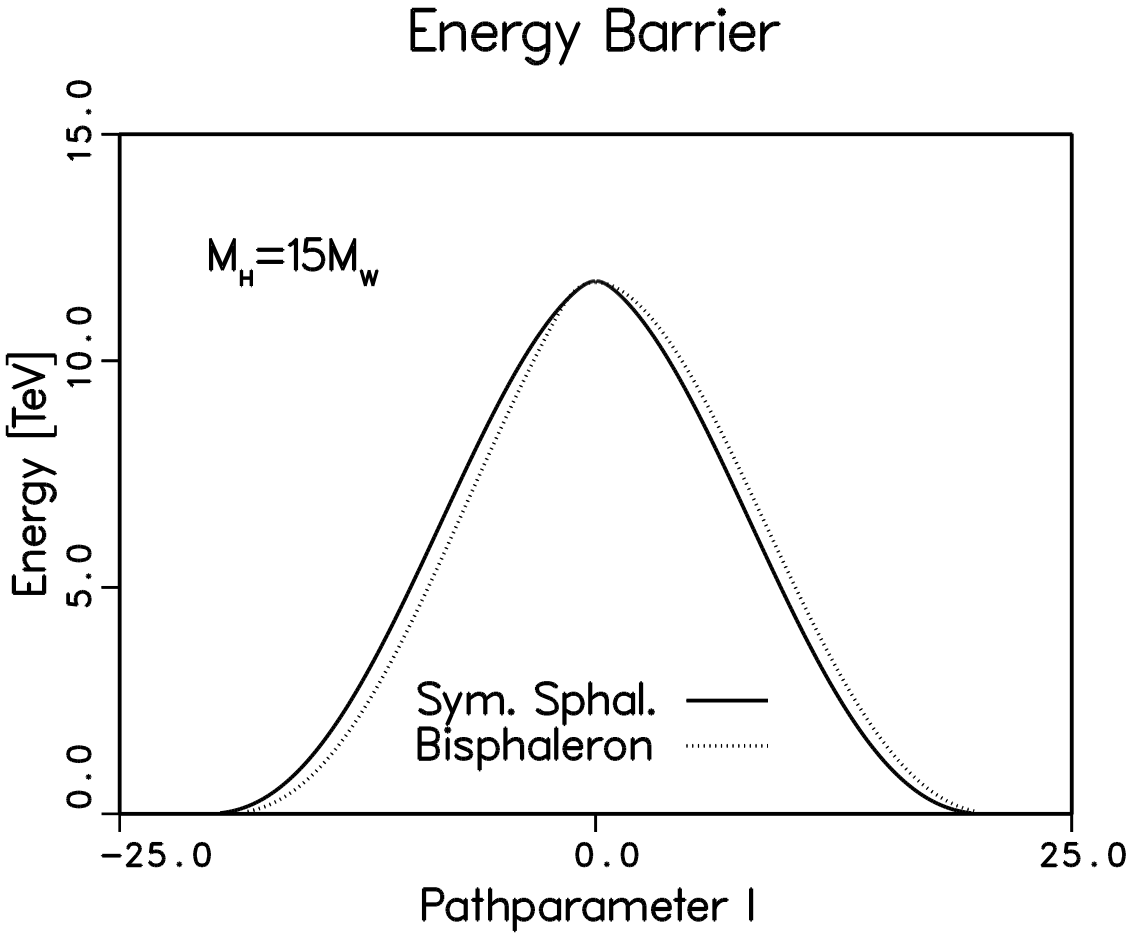
Energy Barrier
15.0
10.0
5.0
0.0
Energy [TeV]
M_H=15M_W
Sym. Sphal.
Bisphaleron
−25.0
0.0
25.0
Pathparameter l

This figure "fig1-5.png" is available in "png" format from:

http://arXiv.org/ps/hep-ph/9409445v2

This figure "fig2-5.png" is available in "png" format from:

http://arXiv.org/ps/hep-ph/9409445v2

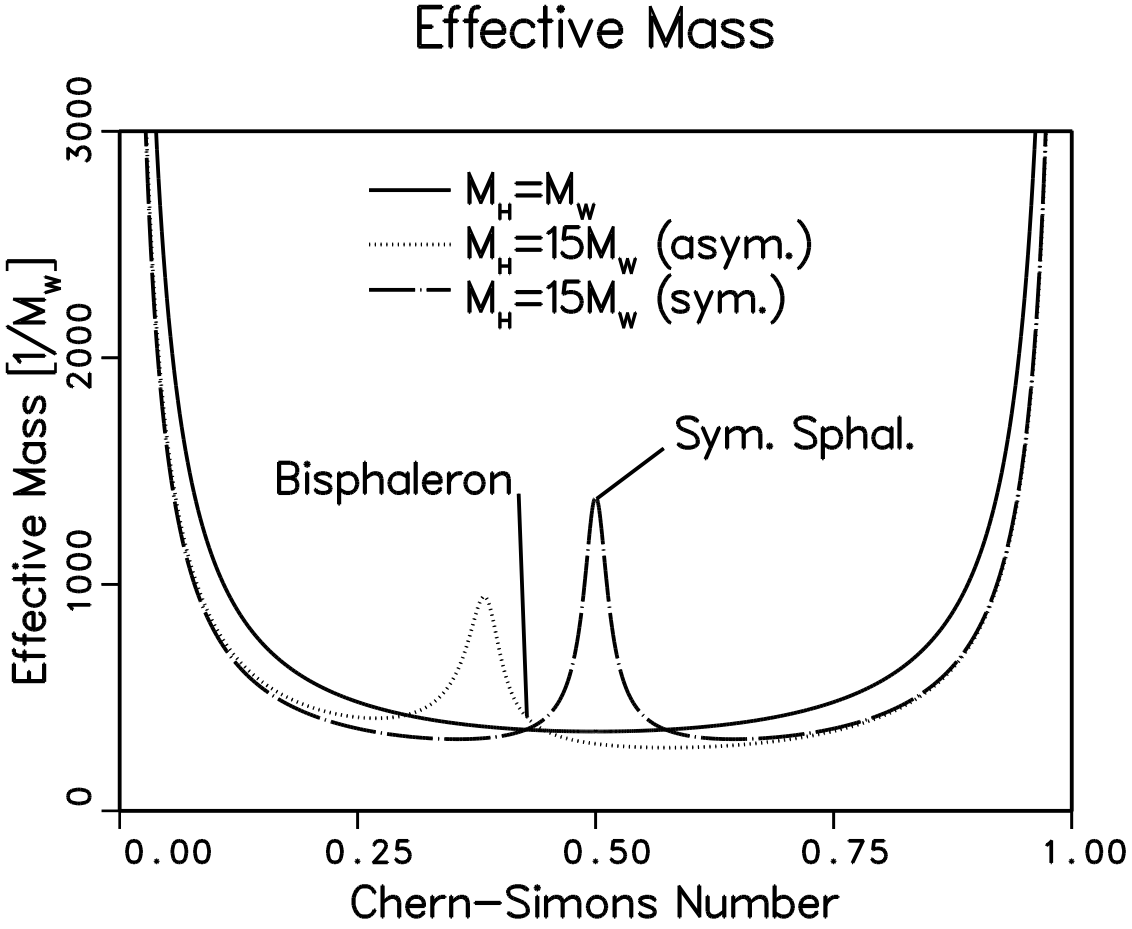
Effective Mass
Effective Mass [1/M_W]
3000
2000
1000
0
M_H=M_W
M_H=15M_W (asym.)
M_H=15M_W (sym.)
Bisphaleron
Sym. Sphal.
0.00
0.25
0.50
0.75
1.00
Chern–Simons Number

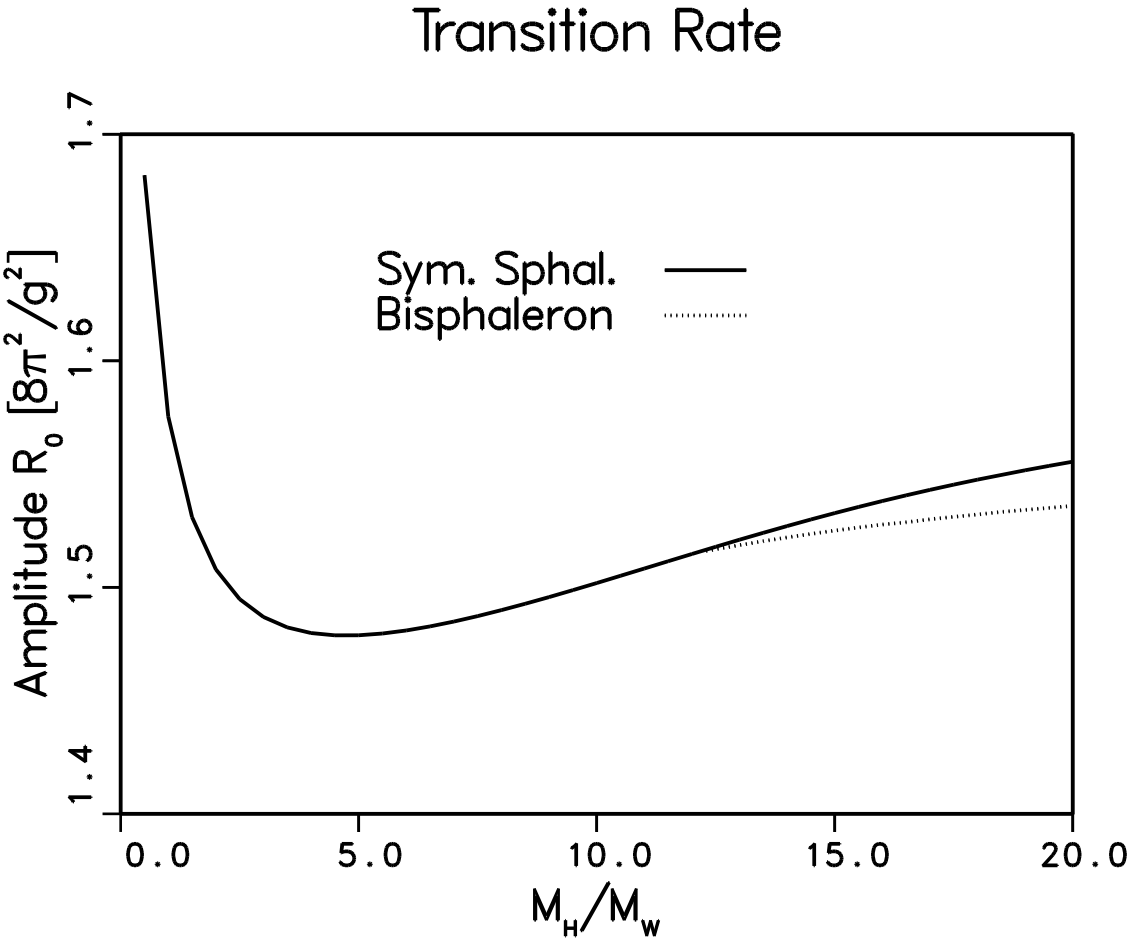
Transition Rate
Amplitude R_0 $[8\pi^2/g^2]$
1.7
1.6
1.5
1.4
Sym. Sphal.
Bisphaleron
0.0
5.0
10.0
15.0
20.0
M_H/M_W

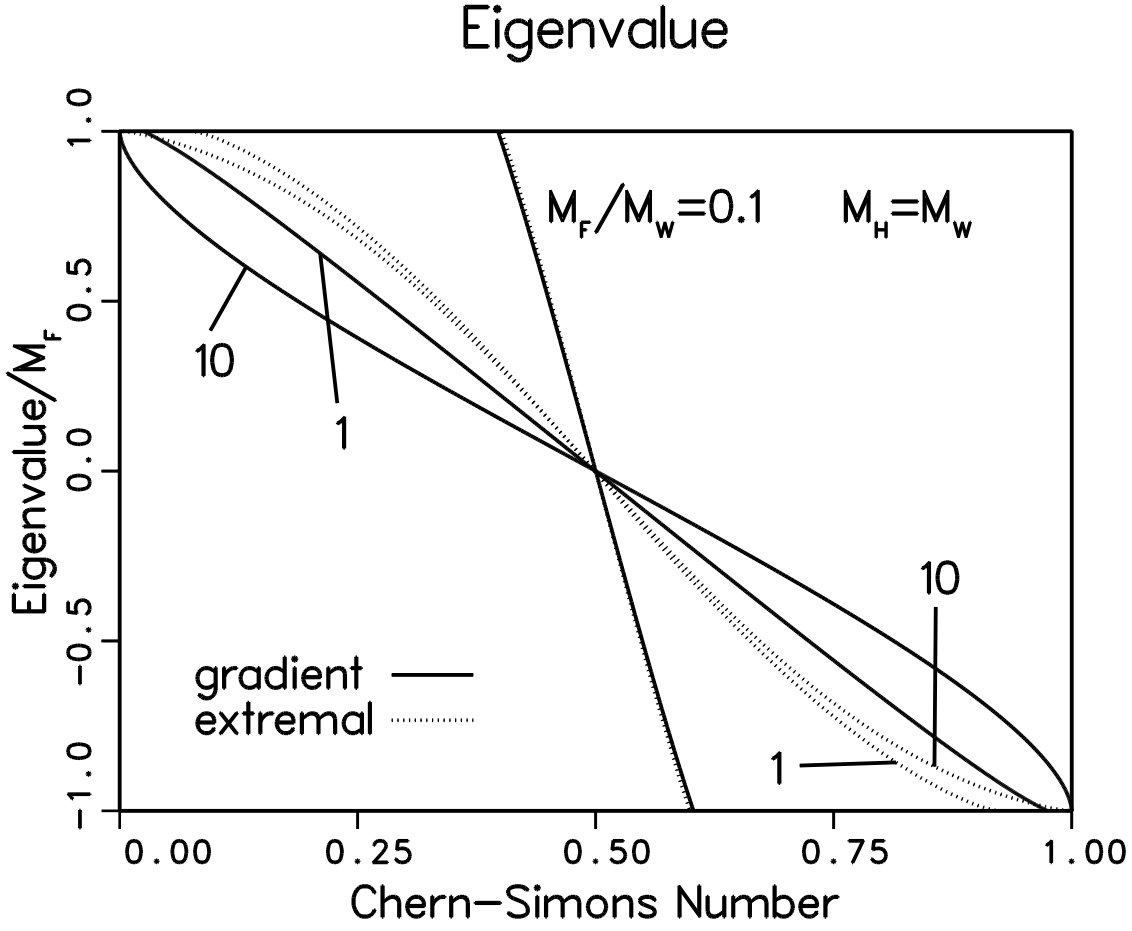
Eigenvalue
Eigenvalue/M_F
1.0
0.5
0.0
-0.5
-1.0
M_F/M_W=0.1
M_H=M_W
10
1
10
1
gradient
extremal
0.00
0.25
0.50
0.75
1.00
Chern–Simons Number

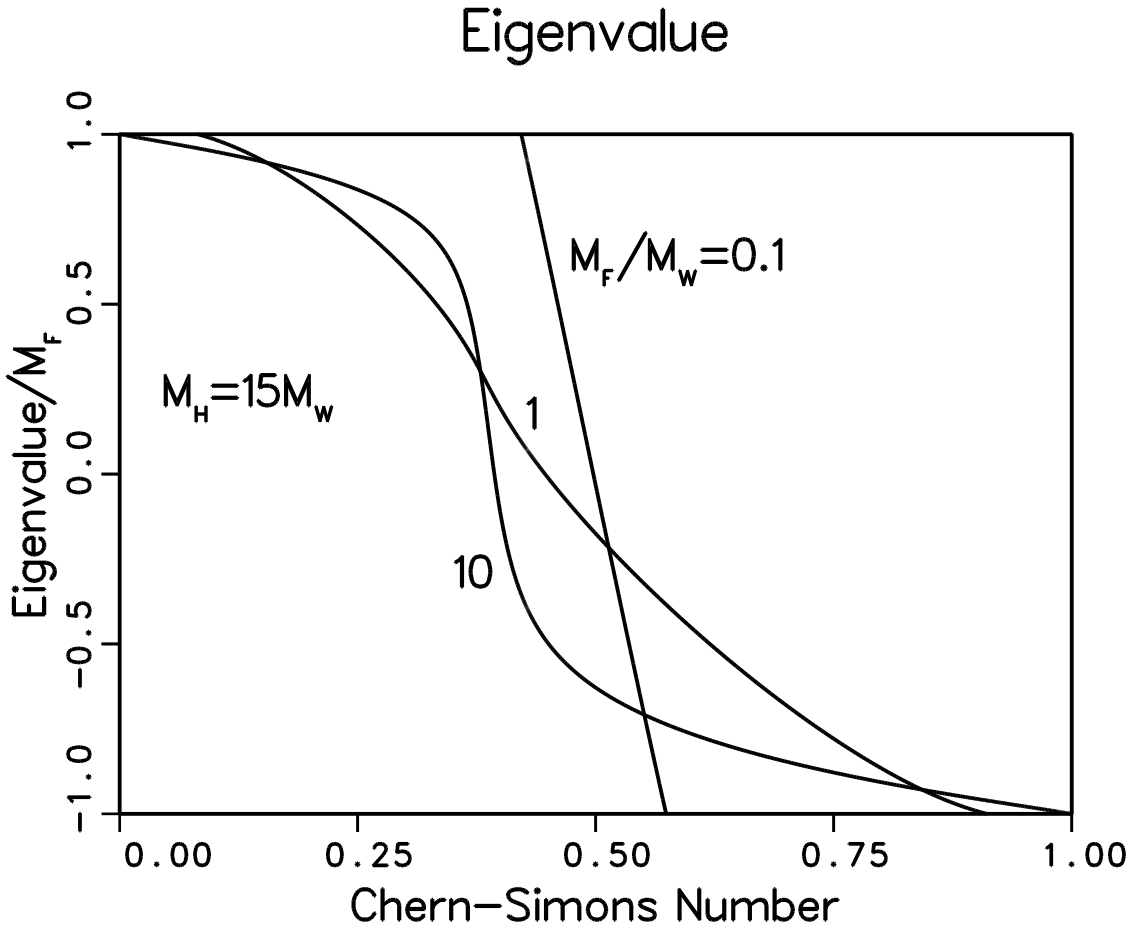
Eigenvalue
Eigenvalue/M_F
1.0
0.5
0.0
-0.5
-1.0
M_F/M_W=0.1
M_H=15M_W
1
10
0.00
0.25
0.50
0.75
1.00
Chern-Simons Number

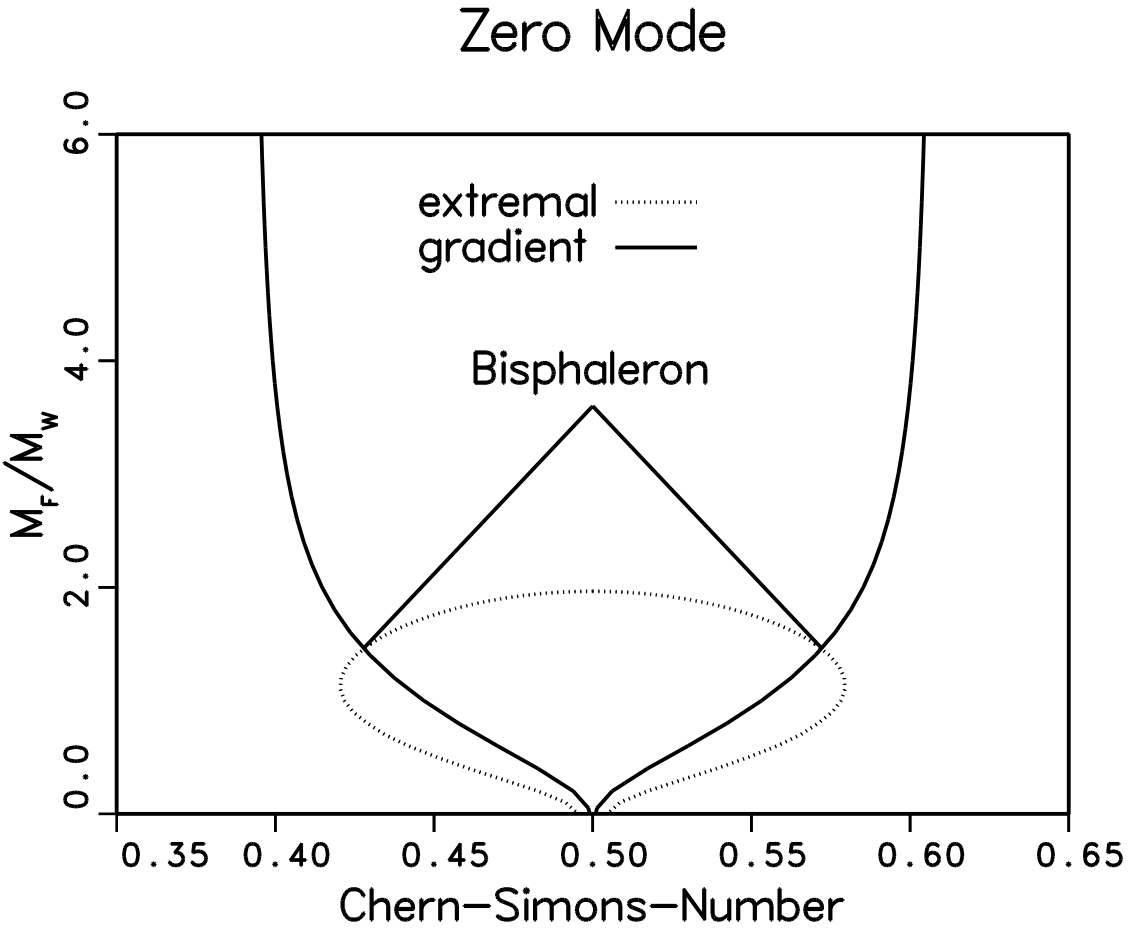
Zero Mode
extremal
gradient
Bisphaleron
M_F/M_w
0.0
2.0
4.0
6.0
0.35
0.40
0.45
0.50
0.55
0.60
0.65
Chern–Simons–Number

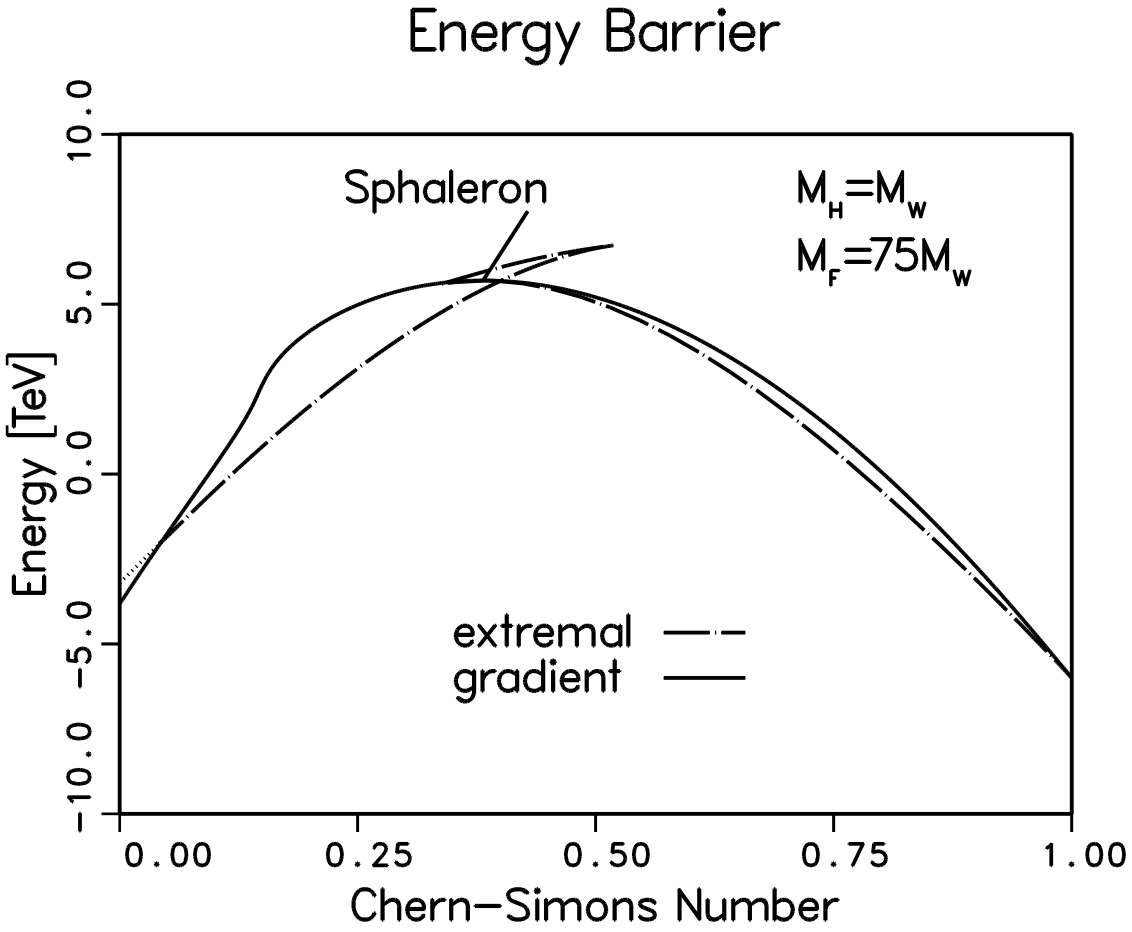
Energy Barrier
Sphaleron
$M_H=M_W$
$M_F=75M_W$
extremal
gradient
Energy [TeV]
10.0
5.0
0.0
-5.0
-10.0
0.00
0.25
0.50
0.75
1.00
Chern-Simons Number

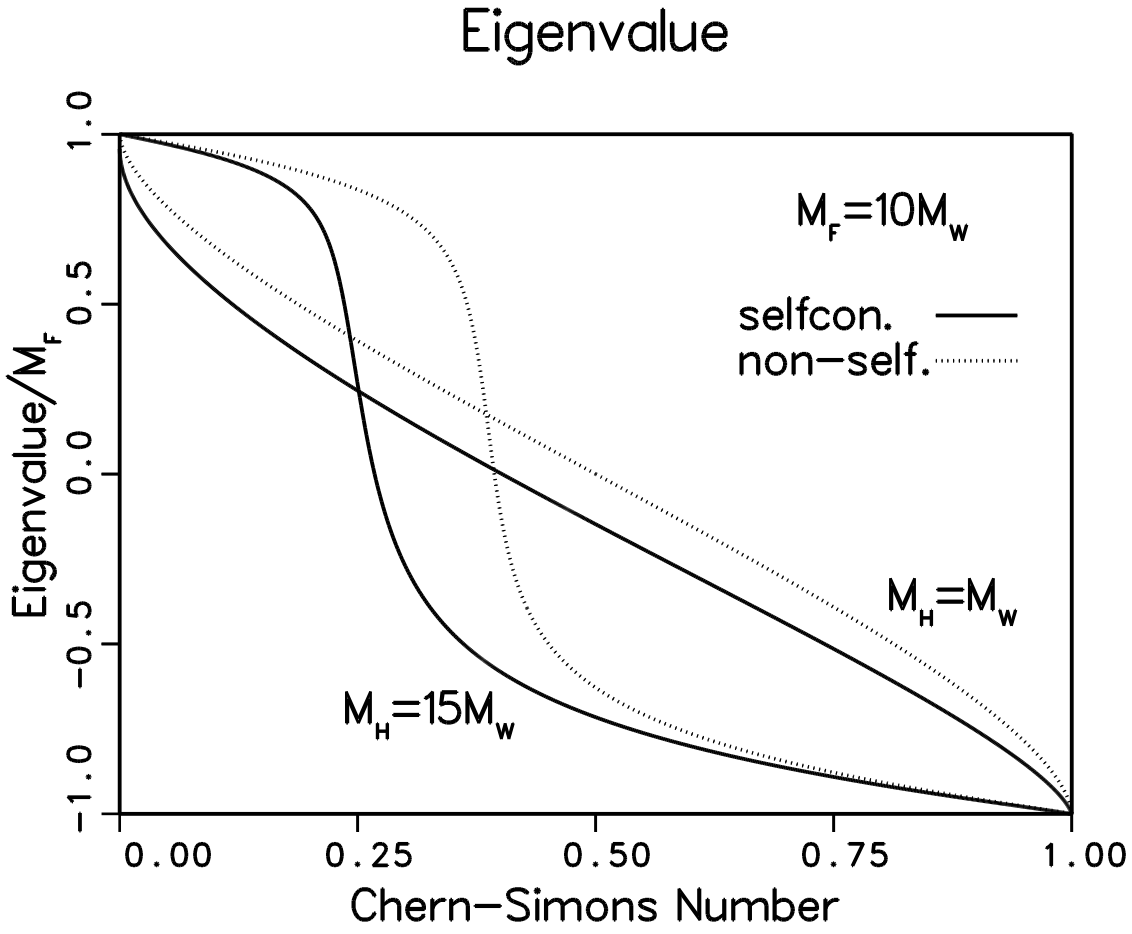
Eigenvalue
Eigenvalue/M_F
1.0
0.5
0.0
−0.5
−1.0
0.00
0.25
0.50
0.75
1.00
Chern−Simons Number
M_F=10M_W
selfcon.
non−self.
M_H=M_W
M_H=15M_W

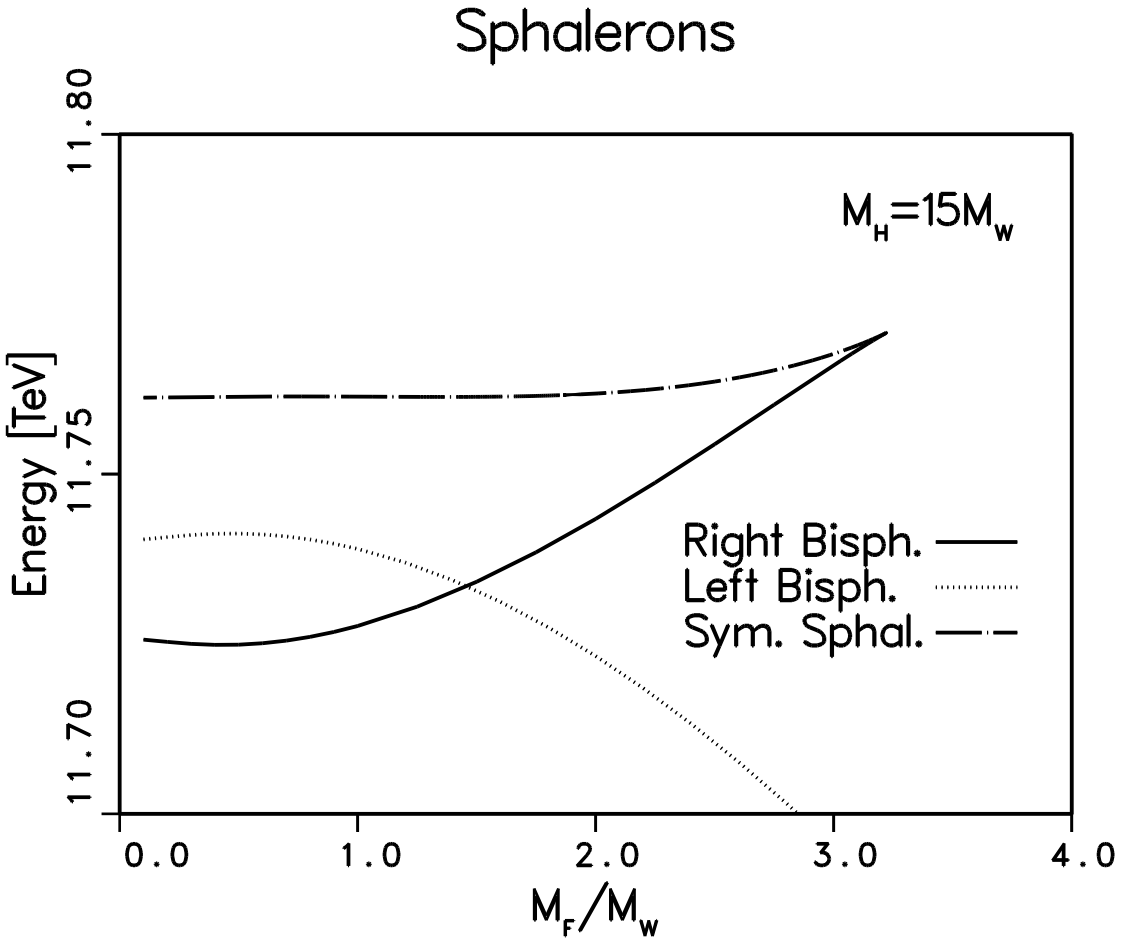
Sphalerons
11.80
11.75
11.70
Energy [TeV]
$M_H=15M_W$
Right Bisph.
Left Bisph.
Sym. Sphal.
0.0
1.0
2.0
3.0
4.0
M_F/M_W